Supporting Information

Improving the Electro-catalytic Activity and Durability of $La_{0.6}Sr_{0.4}Co_{0.2}Fe_{0.8}O_{3-\delta}$ Cathode by Surface Modification

Huijun Chen,[1] Zheng Guo,[2] Lei A Zhang,[3] Yifeng Li,[4] Fei Li,[1] Yapeng Zhang,[1] Yu Chen,[3] Xinwei Wang,[2] Bo Yu,[4] Jian-min Shi,[5] Jiang Liu,[1] Chenghao Yang, [1] Shuang Cheng, [1] Yan Chen [1,6] and Meilin Liu [3*]*

[1] Guangzhou Key Laboratory for Surface Chemistry of Energy Materials, New Energy Institute, School of Environment and Energy, South China University of Technology, Guangzhou510006, China

[2] School of Advanced Materials, Shenzhen Graduate School, Peking University, Shenzhen 518055, China

[3] Materials Science and Engineering, Georgia Institute of Technology, Atlanta, GA 30332-0245, USA

[4] Institute of Nuclear and New Energy Technology (INET), Tsinghua University, Beijing 100084, China

[5] Institute of Nuclear Physics and Chemistry, China Academy of Engineering Physics, Mianyang 621000, China

[6] Guangdong Engineering and Technology Research Center for Surface Chemistry of Energy Materials, School of Environment and Energy, South China University of Technology, Guangzhou, 510006, PR China

*(Y. C.)E-mail address: escheny@scut.edu.cn.

*(M. L.)E-mail address: meilin.liu@mse.gatech.edu.

S1. Pulsed Laser Deposition Target synthesis

LSCF and PrO_2 powder were prepared by nitrate-glycine method, using high purity $La(NO_3)_3•6H_2O$, $Sr(NO_3)_2$, $Co(NO_3)_2•6H_2O$, $Fe(NO_3)_3•9H_2O$ as precursors (Alfa Aesar). The sintering temperature was set to be 1000 °C for 5 h. The GDC and CeO_2 powder were purchased from SOFCMAN, China. PrO_2 (PCO) powder was synthesized by decomposed $PrN_3O_9•6H_2O$ precursor (with additional CeO_2 powder) at 900°C for 5 h. To fabricate PLD targets, powder was grinded with PVB-ethanol solution and uniaxially pressed to form a pellet with diameter of 25mm. The pellet was then sintered to 1300 °C for 6 h in air with a ramping rate of 3 °C /min. The X-ray Diffraction (XRD) pattern for all the target are shown in Fig. S1.

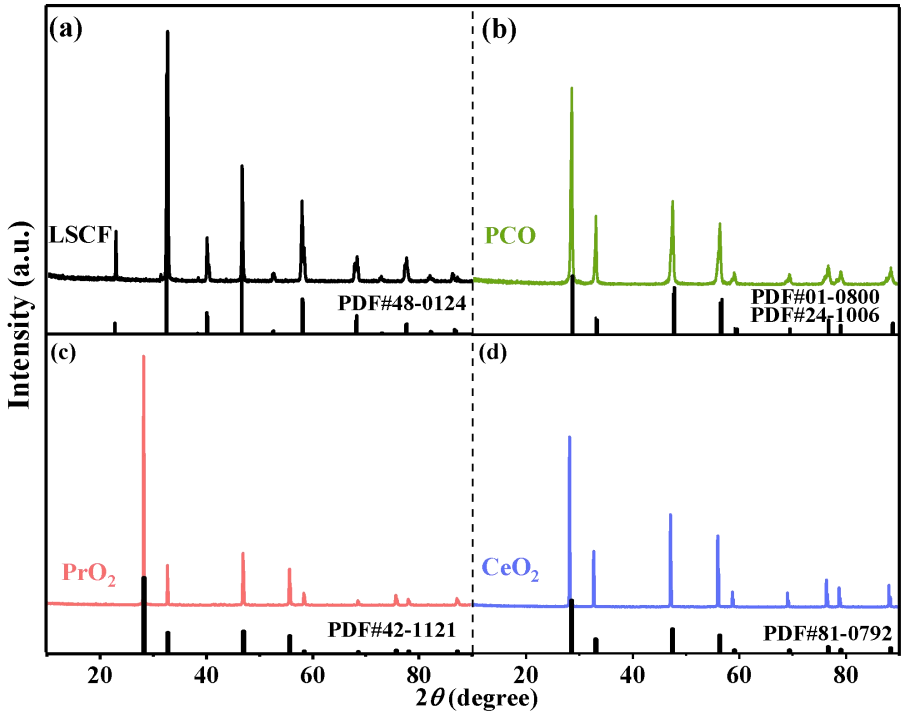

Figure S1. XRD patterns of PLD target after sintering: (a)LSCF, (b)PCO,(c)PrO_2,(d)CeO_2.

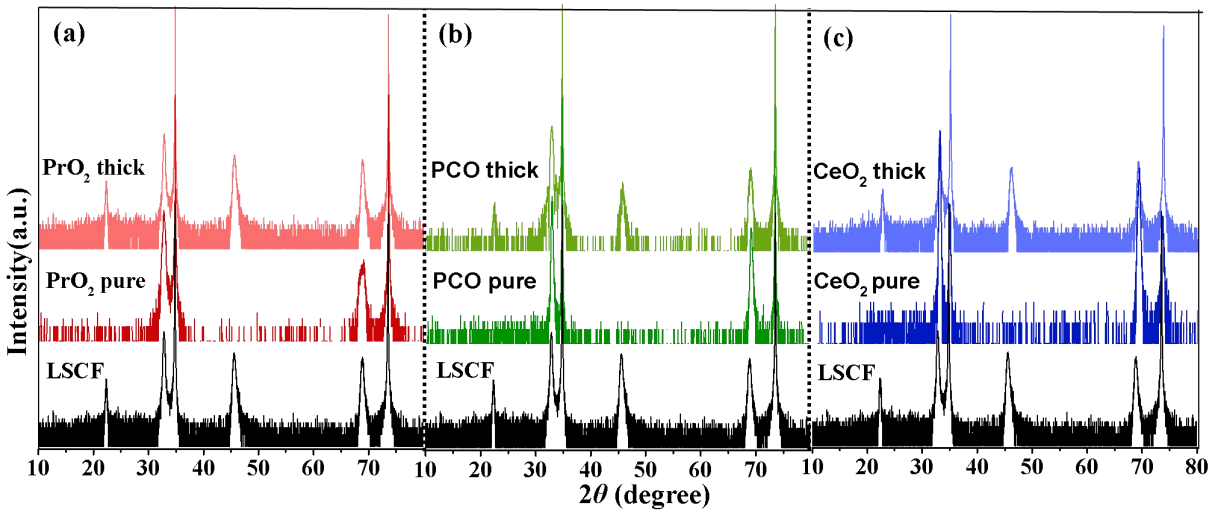

Figure S2. HRXRD patterns of modified LSCF and corresponding single phase reference samples grown by PLD: (a)PrO_2/LSCF, (b)PCO/LSCF, (c)CeO_2/LSCF.

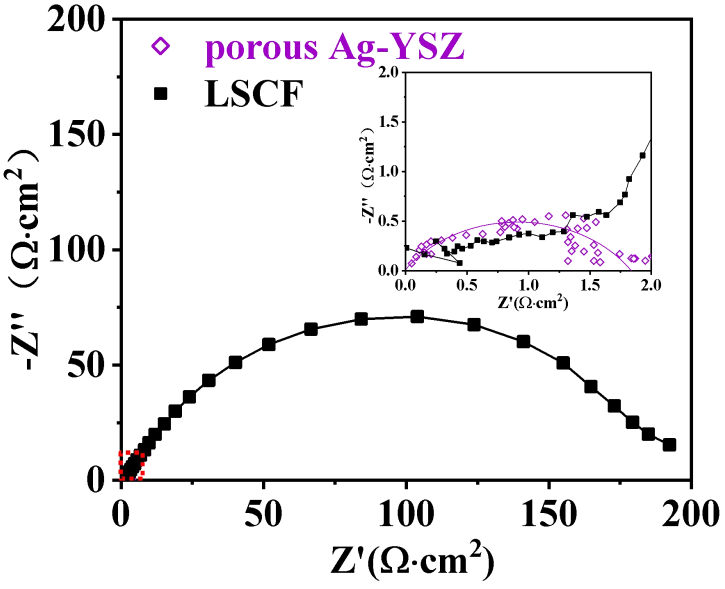

Figure S3. Area specific resistance comparison between porous Ag-YSZ symmetric cell and cell with thin film LSCF as the working electrode and porous Ag-YSZ as the counter electrode at 600 ºC in air.

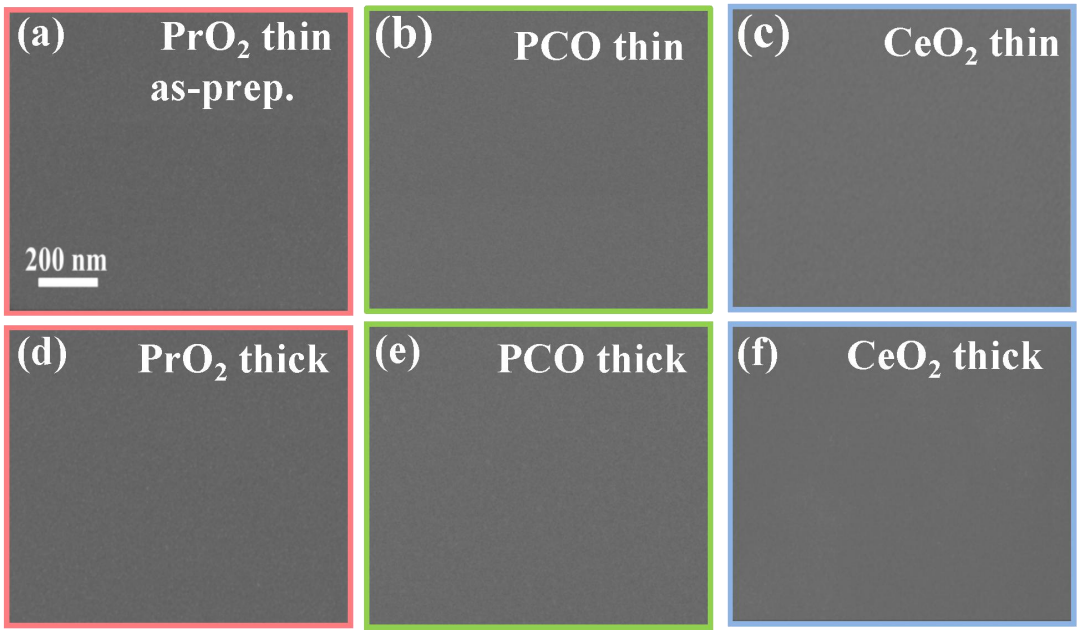

Figure S4. SEM image of the modified LSCF with different thickness in their as prepared states: (a) PrO_2 thin, (b) PCO thin, (c) CeO_2 thin, (d) PrO_2 thick (e) PCO thick, (f) CeO_2 thick.

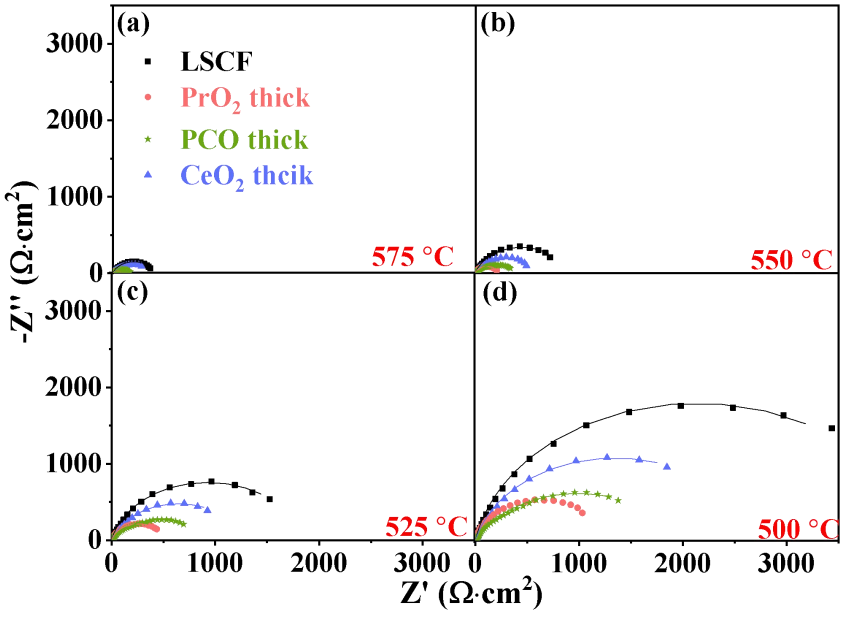

Figure S5. Nyquist plot for the thick (~6nm) $Pr_xCe_{1-x}O_{2-\delta}$ modified LSCF and the reference samples at different temperatures: (a) 575 °C (b) 550 °C (c) 525 °C (d) 500 °C in air

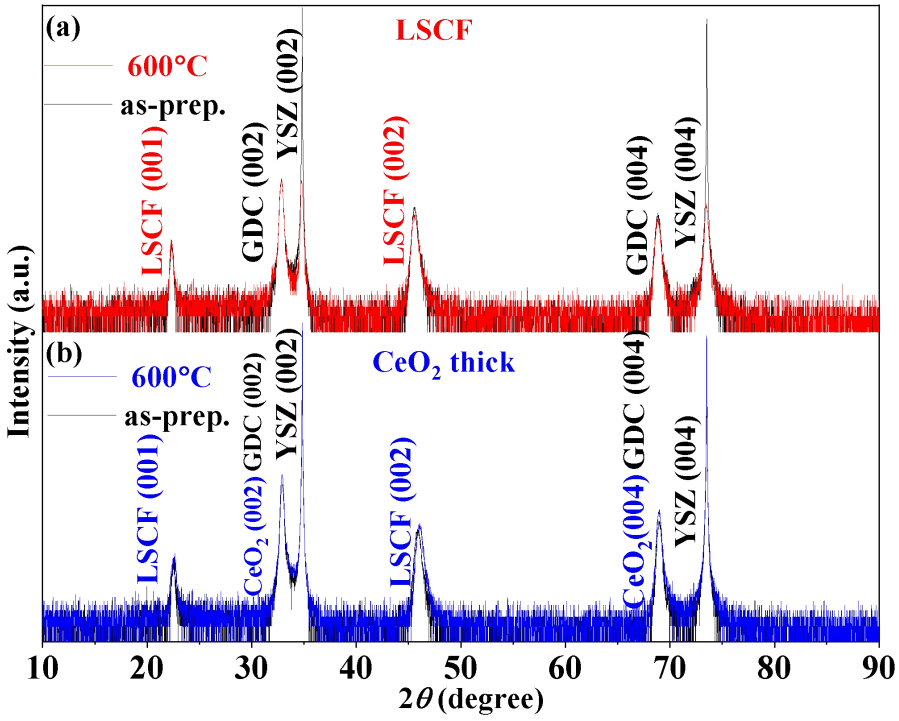

Figure S6. HRXRD patterns of the bare LSCF and the CeO_2 thick/LSCF films in the as prepared states (black line) and after annealing for 3 h in air at 600 °C. (red line and blue line) (a) LSCF and (b) CeO_2 thick/ LSCF

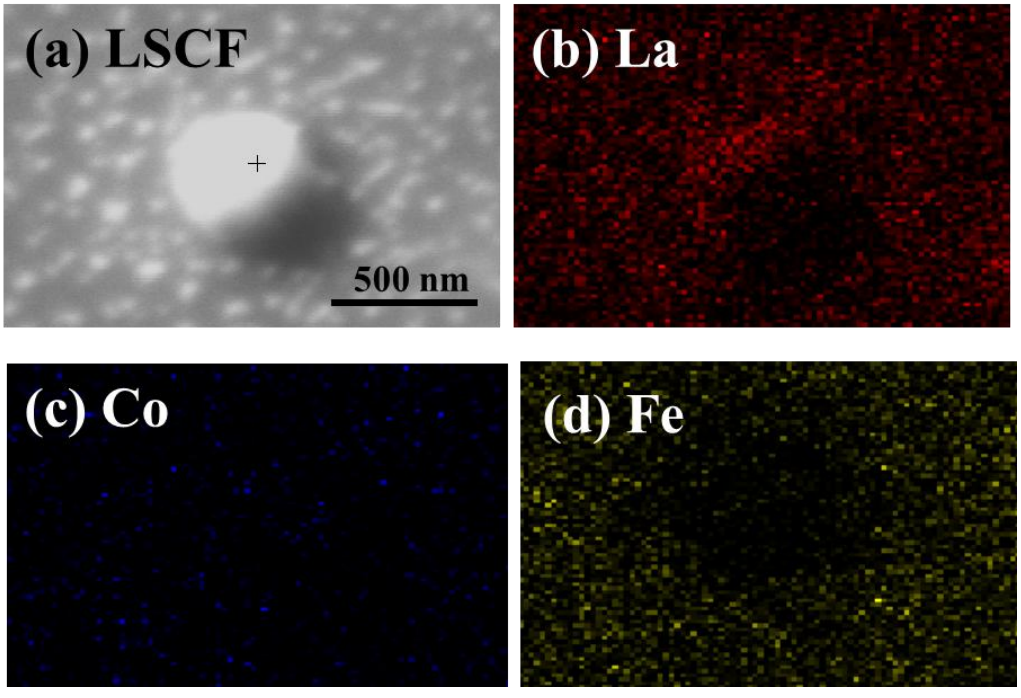

Figure S7. SEM image (a) and the elemental maps from Auger electron spectroscopy for La (b), Co(c), and Fe (d) on LSCF thin film after annealing for 3 h at 600 °C in air. The large particles in image (a) are A-site metal-rich, associated with low contents of Fe and Co.

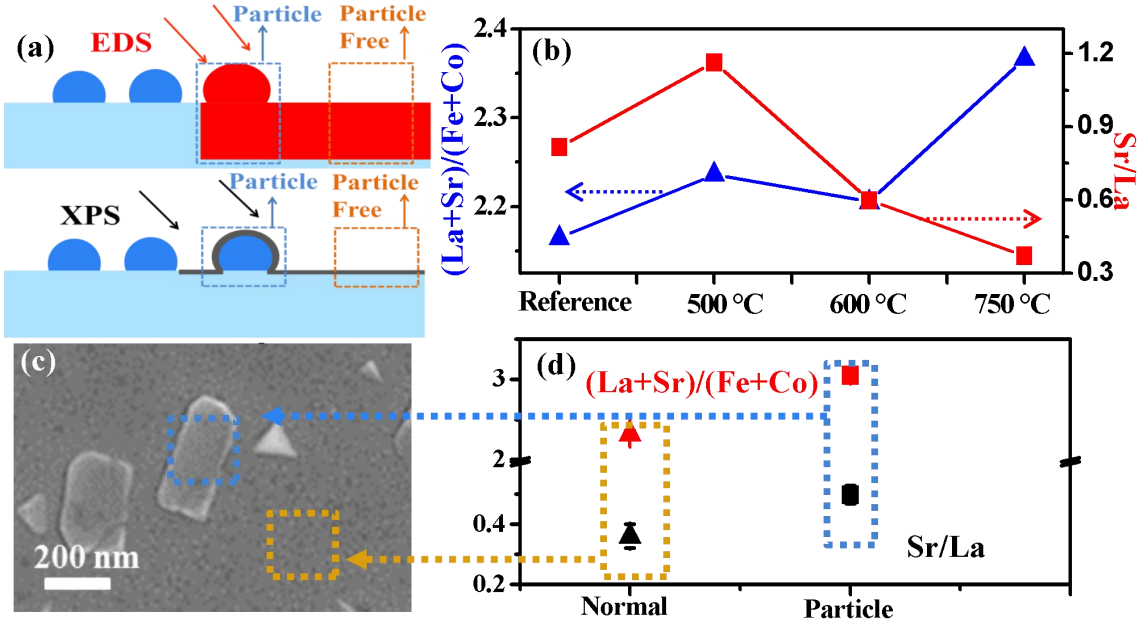

Figure S8. (a) Schematic illustration of different probing depths on thin film surfaces between XPS and EDS analysis technologies (b) Surface composition quantified by XPS for the bare LSCF after annealing at different temperatures in air: reference (before annealing), 500 °C , 600 °C and 750 °C . SEM image of the bare LSCF after annealing at 750 °C in air for 3 h which shows two different regions: region without particle(orange region) and with particle(blue region).(d) EDS quantification of (La+Sr)/(Co+Fe) and Sr/La from regions with particles (blue) and without particles (orange region) as shown in (c).

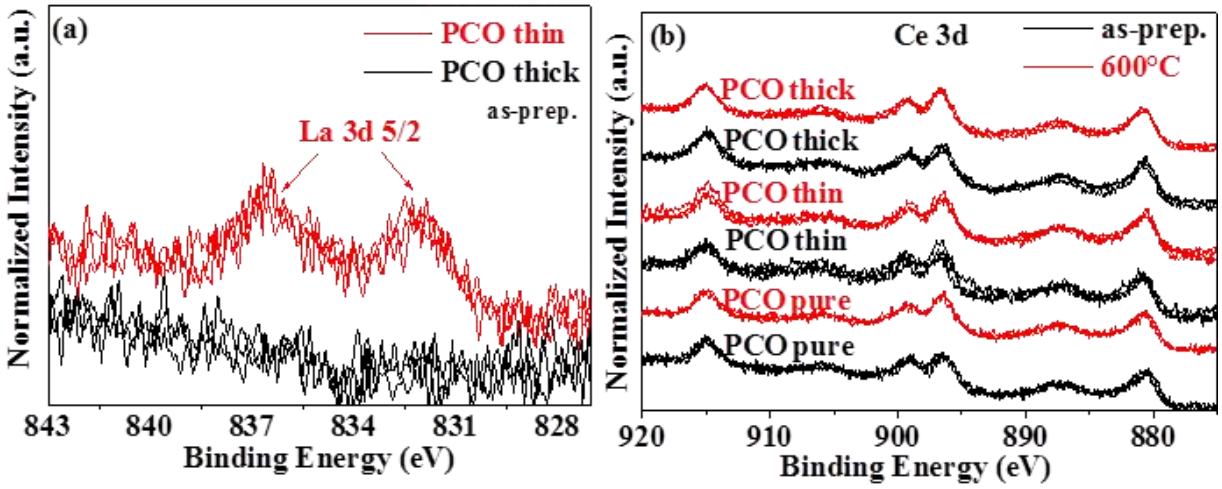

Figure S9. (a) Comparison La 3d5/2 spectra of LSCF modified by PCO layers with two different thicknesses: thin (~2nm) and thick (~6nm). Due to the limit in probing depth, we can not detect La peaks for the LSCF with a thick modification layer; (b) Comparison Ce 3d spectra of PCO single phase and PCO modified LSCF (black line) after annealing in air at 600 °C for 3 h (red line). No noticeable difference is observed.

Table S1. Summary of fitting parameters for Sr 3d peak, including area, position, full width at half maximum (FWHM), $Sr_{non\text{-}lattice}$ to $Sr_{lattice}$ ratio for bare LSCF and modified LSCF with thin $Pr_{1-x}Ce_xO_2$ coating in the as-prepared states and after annealing for 3h at 600ºC.

		LSCF		PrO_2		PCO		CeO_2	
		$Sr_{non\text{-}lattice}$	$Sr_{lattice}$	$Sr_{non\text{-}lattice}$	$Sr_{lattice}$	$Sr_{non\text{-}lattice}$	$Sr_{lattice}$	$Sr_{non\text{-}lattice}$	$Sr_{lattice}$
as prep.	area	4092.56	5556.3	4104	6741.67	512.67	2674.67	3677	18369.33
	Position (3d 3/2, 3d 5/2)	134.30 , 136.05	132.70 , 134.45	133.78 , 135.53	132.38 , 134.13	133.75 , 135.50	132.15 , 133.75	134.17 , 135.92	132.57 , 134.32
	FWHM	1.77	1.32	1.63	1.03	1.37	1.24	1.38	1.28
	$Sr_{non\text{-}lattice}/Sr_{lattice}$	0.73		0.61		0.18		0.18	
600ºC	area	5551.5	4125.5	6975.33	9495.67	1406	7327.67	2074	21055.67
	Position (3d 3/2, 3d 5/2)	133.79 , 135.54	132.19 , 133.94	133.47 , 135.22	131.87 , 133.62	133.62 , 135.37	132.02 , 133.77	133.88, 135.63	132.28, 134.03
	FWHM	1.45	1.25	1.82	1.01	1.56	1.22	1.46	1.5
	$Sr_{non\text{-}lattice}/Sr_{lattice}$	1.34		0.86		0.17		0.1	

Time of Flight Secondary Ion Mass Spectrometry (TOF-SIMS) was used to determine the Sr distribution. The thin film samples were sputtered with a 1 keV O ion beam at 45 angles and the sputtering area was 500 μm×500 μm. A 25 keV Ga primary ion beam was used to analyze the positive ions and the analysis area was limited as 20 μm×20 μm. Representative results of Sr distribution of bare LSCF and surface modified LSCF were shown in **Figure S10**. The bare LSCF surface showed higher Sr concentration than that of the bulk. In contrast, we did not observe noticeable Sr segregation on the surface and near the interface of PCO modified LSCF samples.

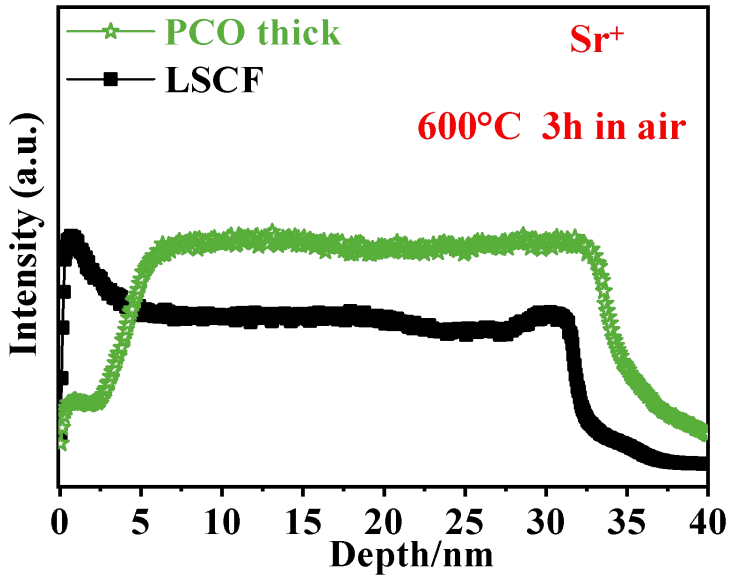

Figure S10. Comparison of Sr distribution of bare LSCF and PCO modified LSCF obtained from TOF-SIMS

S2. DFT calculation of oxygen vacancy formation energy and Sr substitution energy

The oxygen vacancy formation energy E_{vac} is calculated as the energy difference between supercell with one vacancy E_{vacant} with oxygen gas molecule E_{O_2} and perfect supercell without

oxygen vacancy $E_{perfect}$.

$$E_{vac} = E_{vacant} + 0.5\left(E_{O_2} + E_{ob}\right) - E_{perfect}$$

E_{ob} is the well-known over-binding correction on oxygen molecule due to dissatisfied prediction from common LDA/GGA-type exchange-correlation functional, and has the value of 0.92 eV per oxygen molecule in our GGA-PBE prediction. To account for the strong-correlations of *f* electrons, GGA+U method was applied on Ce and Pr with U values of 5 and 6 eV .

Similarly, Sr substitution energy was calculated by replacing one cation with Sr. Due to +2 oxidation state of Sr within dominant +4 oxidation state for host cations, one oxygen vacancy was created near Sr to main charge neutrality of the whole cell. Using CeO_2, PrO_2 and PCO $2 \times 2 \times 2$ supercell as an example:

$E_{Sr-sub} = E(Ce_{31}SrO_{63}) + E(CeO_2) - E(SrO) - E(Ce_{32}O_{64})$ for substituting Ce in CeO_2

$E_{Sr-sub} = E(Pr_{31}SrO_{63}) + E(PrO_2) - E(SrO) - E(Pr_{32}O_{64})$ for substituting Pr in PrO_2

$E_{Sr-sub} = E(Pr_8SrCe_{23}O_{63}) + E(CeO_2) - E(SrO) - E(Pr_8Ce_{24}O_{64})$ for substituting Ce in PCO

$E_{Sr-sub} = E(Pr_7SrCe_{24}O_{63}) + E(PrO_2) - E(SrO) - E(Pr_8Ce_{24}O_{64})$ for substituting Pr in PCO

There is a clear trend that with increasing Pr in the host material, both E_{vac} and E_{Sr-sub} decrease. By forming one oxygen vacancy, two small electron polarons are forming nearby on host cations: two Ce^{3+} in CeO_2, one Ce^{3+} and one Pr^{3+} in PCO, and two Pr^{3+} in PrO_2.